Climatically driven emissions of hydrocarbons from marine sediments during deglaciation

Hill, T.M.[1], Kennett, J.P., Valentine, D.L., Yang, Z.
Department of Earth Science and Marine Science Institute, University of California, Santa Barbara, CA 93106

Reddy, C.M., Nelson, R.K.
Woods Hole Oceanographic Institution, Marine Chemistry and Geochemistry Dept, MS#4, Woods Hole, MA 02543

Behl, R.J.
Department of Geological Sciences, California State University, 1250 Bellflower Blvd. Long Beach, CA 90840

Robert, C., Beaufort, L.
CEREGE-CNRS, Europole Mediterraneen de l'Arbois, BP80, 13545 Aix-en-Provence Cedex 4, France

Classification: Physical Sciences – Geology

17 pages, 4 figures
109 words in abstract; 29,321 characters (text); ~20,000 characters (figures).

[1] To whom correspondence should be addressed. Now at: Geology Department and Bodega Marine Laboratory, University of California, Davis, tmhill@ucdavis.edu, (707) 875 1910.

Abbreviations: SBC, Santa Barbara Channel; ka, ky, thousands of years before present; MIS, marine isotope stage; DIC, dissolved inorganic carbon.

Keywords: Quaternary climate, paleoclimate, hydrocarbon, methane

ABSTRACT

Marine hydrocarbon seepage emits oil and gas, including methane (~30 Tg CH_4/year), to the ocean and atmosphere. Sediments from the California margin contain preserved tar, primarily formed via hydrocarbon weathering at the sea surface. We present a record of variation in the abundance of tar in sediments for the past 32ky, providing evidence for increases in hydrocarbon emissions prior to and during Termination IA (16-14 ka) and again over Termination IB (11-10 ka). Our study provides the first direct evidence for increased hydrocarbon seepage associated with deglacial warming via tar abundance in marine sediments, independent of previous geochemical proxies. Climate-sensitive gas hydrates may modulate thermogenic hydrocarbon seepage during deglaciation.

INTRODUCTION

Dramatic changes in atmospheric methane concentrations have occurred on glacial-interglacial and millennial time scales and are typically attributed to varying biological production of CH_4 in wetlands (1). However, contributions from "geologic" methane sources, including thermogenic hydrocarbons in hydrates and/or sedimentary reservoirs, remain largely unknown. Quantifying past and present emission rates of methane from marine and terrestrial hydrocarbon sources is critical in understanding the contribution of methane to the atmosphere from these natural sources (2,3).

Marine hydrocarbon seepage emits oil and gas, including methane (~30 Tg CH_4/year globally), to the ocean and atmosphere (3). In the southern California region, over 200

persistent hydrocarbon seeps have been reported, with several in Santa Barbara Channel (SBC; Fig. 1). Seepage in this region is controlled by faults and anticlines overlying a reservoir of thermogenic hydrocarbons derived primarily from the Monterey Formation, which is the source and reservoir rock (4). Most identified seeps in this region are located at shallow water depths (20-60m), but locations of active seepage and seepage "indicators" (pockmarks, mud volcanoes, tar mounds) have also been identified between 300-590m (Fig.1; 5,6). At modern seeps in SBC, all observed petroleum seepage is closely associated with gas emission; in fact, seepage of methane gas far exceeds that of petroleum (8,9; Boles, J., pers.comm). While there is significant tar/hydrocarbon accumulation at localized sites of seepage, surface-ocean oil slicks can extend for more than 10 km from their source in the SBC region (2,8,9). As oil at the sea surface is biologically degraded and volatile components evaporate, a negatively buoyant tar residue forms, which is eventually deposited on beaches and in basin sediments (2). However, general observations indicate little or no long-term accumulation of tar on these beaches, as the tar is removed from the shoreline within the timescale of tidal cycles.

In the SBC region, existing sediment geochemistry records, pockmark ages and changing geochemical composition of fault-vein calcites provide evidence for variable hydrocarbon emissions during the late Quaternary (10-13). Negative $\delta^{13}C$ shifts recorded in planktonic foraminifera during rapid interstadial warming events in SBC have been previously interpreted as destabilization of methane hydrates and release of methane to the water column and atmosphere (11). In addition, $\delta^{13}C$ values and radiocarbon dating of

foraminifera from a pockmark near modern seeps in SBC suggest gas emissions during the last 25 ky (12). U-Th dating and $\delta^{13}C$ composition of fault vein calcites indicate intermittent hydrocarbon seepage in this area for the past ~500 ky (10). Sediments from Ocean Drilling Program Site 1016, offshore Pt. Conception (northwest of SBC) record changing concentrations of petroleum compounds over the past 150 ky (13). This record indicates an increase in petroleum compounds (hopanes) preserved in offshore sediments during major deglacial warming episodes (13). Collectively, these records suggest that hydrocarbon seepage on the California margin has been variable during the late Quaternary. For the first time, we employ changing abundance of tar in marine sediments as a direct proxy for hydrocarbon seepage in the latest Quaternary.

Santa Barbara Channel overlies the northernmost physiographic basin of the California Continental Borderland. The 590-m-deep Santa Barbara Basin is bounded by a deep western and shallower eastern sill and encompasses nearly 5000 km^2. A persistent gyre dominates the western end of the channel for much of the year, influenced by short-term upwelling and by the southward-flowing California Current and opposing Southern California Countercurrent. The cores studied in this investigation were taken from the *R/V Marion Dufresne*, in the central basin (569 m) and the eastern end of the basin (481 m; Fig 1). Sedimentation rates at these locations were relatively high and constant for the past ~30 ky averaging 130cm/ky.

RESULTS

Marine sediments are routinely microscopically examined to investigate the sand-sized fraction, including microfossils. While investigating rapid climate change in cores from SBC we observed variable abundances of tar in the sedimentary record. To quantify the occurrence of tar, an index was established to reflect the percent of sand grains (>63μm) observed under light microscopy composed of and/or covered by tar (Fig. 2). The quantitative visual analysis and generation of the "tar index" was then utilized to target specific intervals for additional analyses. As such, variations in the weight percent of tar were determined in selected samples via solvent extraction (see online supplementary information for methods). The tar index was preferred over gravimetric analysis for several reasons: it is less labor intensive and allows for greater sampling frequency, is non-destructive, and provides immediate integration of tar observations with other sedimentary parameters. While hydrocarbon emissions are subject to dispersal and degradation, the tar index utilizes the fraction of hydrocarbons that remain preserved in the geologic record. In addition to the quantitative tar index, tar from seven sediment samples was combined and analyzed using comprehensive two-dimensional gas chromatography (GCxGC), which confirmed that it is similar to tar found on modern Santa Barbara beaches (see online supplementary information; 9).

A planktonic foraminiferal (*Globigerina bulloides*) $\delta^{18}O$ record for both cores is presented for climatic context. The chronology of both cores is based upon multiple correlations to the established record at ODP Site 893 (Fig.2; 14).

The tar index (Fig. 2) reflects varying abundance of tar in SBC sediments over the last 32ky. A "background" abundance (Index 1-2) of tar is apparent, consistent with modern observations of persistent hydrocarbon seepage. The abundance of tar in MD02-2503 increased during several intervals. Tar abundance episodically increased from 31 to 26 ka, in association with the stadial/interstadial climatic instability of Marine Isotope Stage (MIS) 3, as apparent in the $\delta^{18}O$ record. Distinct increases are observed again from 16.2 to 14.2 ka, coincident with deglacial warming and the onset of the Bølling-Allerød chronozone (B/A); this includes the interval of greatest tar abundance (~15 to 14ka). Finally, tar abundance increased again over the transition into the early Holocene (~11ka). The tar index record for MD02-2504 exhibits similar tar abundance oscillations, with increased tar prior to and during Termination IA (16 to 14 ka) and again over Termination IB (11-10 ka). In both cores, the tar index indicates decreased tar abundance during the Holocene compared to the glacial termination.

DISCUSSION

We interpret the tar investigated in this study as reflecting hydrocarbon weathering and deposition that is synchronous with the sedimentation at the core sites, not seepage that has migrated upward through the sedimentary column. Several lines of evidence support this interpretation. First, as discussed above, petroleum from the Monterey Formation that floats to the surface is readily weathered in oil slicks to the point of becoming negatively buoyant – presumably because of its unusually high resin, asphaltene and heteroatom content (2, 17). Consistent with this observation, hydrocarbon compounds have previously been detected in sinking particles collected in sediment traps in Santa Barbara

Basin (18). This mechanism provides the source for tar throughout the SBC, including shoreline and deeper basin sediments. Second, there is no indication that changes in characteristics of the sedimentary record correlate with changes in the tar index. For example, changes in lamination/bioturbation of SBC sediments are not associated with tar index variability; rather, a distinct delay exists (~2 ka) between the timing of increased tar index values and the onset of laminations during deglaciation. This observation rules out a sedimentary-driven process, such as an increase in lamination strength providing a "seal" for upward migration of hydrocarbons. Finally, regardless of tar index values, the tar was consistently observed accreting to regular marine sedimentary material, including pelagic biogenic components, suggesting that the tar was deposited contemporaneously with these sediments.

We interpret the variations in the relative abundance of tar as a proxy for changing emissions of hydrocarbons, including methane. As stated previously, methane gas emission is closely associated with petroleum seepage in SBC (8,9). In turn, variability of active hydrocarbon fluid flow has been inferred previously from fault calcites in the Santa Barbara region over the past 500 ka (10). These observations are consistent with our interpretations of variability in hydrocarbon seepage in this region. Based upon the tar index, hydrocarbon emissions clearly increased during deglacial warming (16-14 ka, and 11-10 ka; Fig. 2). In contrast, the Holocene exhibits relatively low hydrocarbon emission rates. While increased variability in seepage was associated with MIS 3, the most conspicuous hydrocarbon emissions occurred during the abrupt climate changes of Terminations IA and IB.

Many previous investigations of seepage in this region have focused on shallow water depths (20-60m). These seepage sites are too shallow to contribute to the tar index record, which indicates increased hydrocarbon seepage during early deglacial warming, when sea levels were >100m lower. However, locations of active seepage and seepage "indicators" have been identified in the modern basin between 300-590m (Fig. 1; 5, 6). These observations provide ample evidence for seepage sites within the depth range required to explain the tar index record. In addition, hydrocarbon deposits are common along the California coast, and the tar index may incorporate hydrocarbons originating from outside of SBC (19). Comparison of the tar index between the two cores indicates that the deeper site (MD02-2503) has higher index values during the deglacial episode. This may reflect location of seepage sites, or that basin circulation acted to focus tar at the central site.

We consider several mechanisms that could change seepage rates and/or accumulation of hydrocarbons. Sea level could potentially affect the locations and rate of seepage: during lower sea level of the last glacial, marine seepage might have increased due to reduced hydrostatic pressure at the sediment-water interface and exposure of seeps on continental shelves (20). This process has been observed on short time-scales: hydrocarbon seepage rates in the SBC are partially controlled by changes in hydrostatic pressure during tidal cycles (21). However, sea level could not have been the primary mechanism that controlled past hydrocarbon emissions as the deglacial transgression was a time of *increasing* tar abundance in basin sediments. Alternatively, sea level rise and transgression may have 'activated' shallow seepage sites by reconnecting them with the

ocean; however, sea-level curves indicate only modest sea level rise (15-20m) from 19-14.6ka, with much of sea level change following the abrupt deglacial warming (22). Thus, sea level apparently did not play an important role in increasing hydrocarbon emissions during the deglaciation. Increased storminess during deglaciation may have mobilized existing tar deposits; however, there is no sedimentologic evidence for these processes, such as the presence of sand layers (23). The restriction of the basin due to lowered sea level may have acted to concentrate tar deposition near the basin center, but this alone is unlikely to account for a threefold increase in % tar (Fig. 3), or for the association with deglaciation. Therefore, we look for mechanisms beyond sea level, remobilization of hydrocarbon deposits, and basin restriction to explain the deglacial increase in tar abundance.

The increase in tar abundance may reflect subsurface interaction between thermogenic hydrocarbons and methane hydrate, which is widely present on continental margins, dependant upon water temperature, pressure, and the presence of thermogenic or biogenic methane (Fig. 4; 24). Gas hydrates commonly overlie or occur near thermogenic reservoirs, such as in the Gulf of Mexico and the western margin of North America, with subsurface connectivity between the reservoirs (25, 26). Therefore, factors influencing the stability of hydrates could influence thermogenic hydrocarbon migration. We suggest that hydrate instability, which may be sensitive to Quaternary climate change, modulated hydrocarbon fluxes via several potential mechanisms: the upward migration of hydrocarbons through destabilized hydrates, the production of free gas pathways within hydrate stability zones, and sediment slumping/landslides that exposed new hydrocarbon

conduits (7, 27, 28). In essence, methane hydrates may act as a climate-sensitive valve system for thermogenic hydrocarbons.

We examine gas hydrate stability during three intervals, each marked by different pressure/temperature conditions, to assess the potential for hydrate destabilization and inferred "activation" of petroleum reservoirs (Fig. 1 and 4). Estimates of gas hydrate stability in Figures 1 and 4 are based upon assumptions detailed below. Gas hydrate stability was estimated utilizing (29), with estimates of changing SBC bottom water temperatures from (16).

First, during the Last Glacial Maximum (**Scenario 1**; 18 ka) when bottom water temperatures were 2°C, and sea level was ~120 m below present, gas hydrate stability occurred below ~420 m in the SBC. During Termination IA (**Scenario 2**; 16-14 ka), when bottom water temperatures had warmed by ~2°C and sea level had risen by ~15 m (22), gas hydrate stability existed below 480 m. Finally, in the early Holocene (**Scenario 3**; ~9 ka), when bottom waters had warmed by an additional ~2°C, and sea level had risen to modern levels, gas hydrate stability was similar to scenario 1, residing below ~425 m.

Thus, during the last glacial maximum and the Holocene, a combination of specific temperature and sea level conditions led to similar gas hydrate stability in the SBC (Fig. 1). During the LGM and Holocene (scenarios 1 and 3), almost half of the deep SBC waters were within the gas hydrate stability field; in contrast, during Termination 1A (scenario 2) the majority of the deep SBC was outside of the stability field (Fig. 4).

During deglaciation, the depth zone and spatial extent of gas hydrate stability in the basin were reduced, promoting destabilization of existing hydrates. We find that gas hydrates in SBC would have been most susceptible to destabilization during early deglaciation, due to the dominant effect of temperature on gas hydrate stability during this time period.

Gas hydrates and hydrocarbon reservoirs elsewhere along the California coast may have responded similarly. For example, seepage near Pt. Conception (northwest of SBC) may have contributed to the tar preserved in SBC sediments via transport in the California current (19). Changes in concentrations of petroleum compounds (hopanes) from ODP Site 1016 (3846m, on the continental slope offshore Pt. Conception) correlate with major shifts in climate, with the largest peaks over major deglacial warming during Terminations I and II (13). These hopane peaks were originally interpreted to reflect major reworking of tar from mounds on continental shelves during marine transgression (13). Although sea level transgression over the shelf may have led to recycling of tar, given the new evidence provided by the higher resolution SBC records, this mechanism now seems unlikely to account for observations from the lower resolution Site 1016 record, (~5 cm/ky). We interpret the Site 1016 record as strongly supportive evidence for hydrocarbon seepage during deglacial warming and the clear relationship between climate change and marine seepage. The Site 1016 record indicates that direct evidence of hydrocarbon seepage is not limited to restricted basins such as the SBC, and is instead a regional-scale process.

Intriguingly, the most significant peak in tar abundance (over Termination IA) overlaps with a distinctive negative $\delta^{13}C$ shift recorded in planktonic foraminifera from these sites (see online supplementary information; 16). From 14.6 ka to at least 12 ka, the $\delta^{13}C$ values of *G. bulloides* in MD02-2503 and MD02-2504 shift from an average of –0.5‰ to –2.0‰, with the most dramatic shift at 14.6 ka. This provides further evidence of a $\delta^{13}C$-negative source to the dissolved inorganic carbon (DIC) pool at this time, consistent with methane seepage.

Modern global methane seepage from marine sources to the atmosphere is estimated to be ~30 Tg/year, reflecting 15% of the natural (non-anthropogenic) sources (3). The tar index and % tar records demonstrate at least three times more tar in the SBC during the deglaciation relative to the modern. Modern seepage rates from one source in the SBC (Coal Oil Point) average ~0.029 Tg CH_4/year[2]; based upon this we estimate that total methane seepage in SBC likely exceeds 0.10 Tg CH_4/year. Thus, methane seepage in this area during the deglaciation may have reached 0.3-0.4 Tg CH_4/year. If this change in tar abundance is scaled to estimate *global* marine methane flux, seepage would have increased to ~90 Tg CH_4/year, totaling ~50% of the estimated total methane source during the deglaciation (175-185 Tg CH_4/yr during the Bølling transition; 30). Such a large estimate would require equivalent and synchronous response from methane seeps around the world, which is unlikely. While little is known of past global hydrocarbon seepage variability, this study indicates that if similar processes occurred broadly on continental margins, this would represent a significant source of methane to the atmosphere. Thus, these findings suggest that interactions between the hydrocarbon and

hydrate reservoirs may increase the amount of available methane that can be transmitted to the ocean and atmosphere during climatic warming.

METHODS

Tar in these sediments is readily identified as black-brown, sometimes semi-translucent, and frequently observed in aggregates or accreting on to other particles. The tar index reflects the percentage of sand grains composed of or coated by tar as determined using stereoscopic light microscopy. Additional information on methods is provided in the online supplementary material.

Tar Index 1: Tar is rare. Small flakes accreting to other particles may be observed, but on less than 10% of the sand-sized grains.

Tar Index 2: 20% of the grains are composed of and/or covered by tar.

Tar Index 3: 30% of the grains are composed of and/or covered by tar, rarely observed in aggregates

Tar Index 4: 40% of the sand-sized grains are composed of and/or covered by tar; tar/sand aggregates (<1mm) are present.

Tar Index 5: 50% of the sand-sized grains are composed of and/or covered by tar; large (>1mm) tar/sand aggregates present.

For consistency, one investigator determined the tar index for all of the samples in this study and then replicated approximately 50% of the samples. A second investigator replicated the tar index for approximately 30 samples to confirm tar abundance estimates and minimize operator error. In total, 10-15% of samples required adjustment by 0.5-1 index point upon replication. Half measures (e.g., 3.5) were used when tar was observed between index points. Sample resolution

for the tar index and isotopic analyses is 5-10cm for most of the core, with two brief high-resolution intervals (1cm) from 14.7-14.2 ka and 10.8-10.6 ka.

For determination of % tar, a selection of bulk sediment samples (>63mm fraction) were weighed and then treated in a solution of acetone and dichloromethane (1:1). The tar (in solution) was decanted from the sediments and weighed after solvent removal in a fume hood at room temperature.

Between 10-25 *G. bulloides* specimens from the >250μm fraction were analyzed for stable isotopes. Samples with tar accreting to foraminiferal specimens were avoided for isotopic analyses. Samples for isotopes were cleaned by sonication in methanol and roasted under vacuum for 1 hour. Isotopic analyses were conducted using a Finnigan/MAT 251 light stable isotope mass spectrometer, with instrumental precision of <0.09‰ for both carbon and oxygen isotopes. All data are expressed as standard delta (δ) notation in per mil relative to PeeDee Belemnite Standard, related by repeated analysis of NBS-19.

Acknowledgments
The authors thank the Institut Paul-Emile Victor (IPEV), Yvon Balut, and the Scientific Party of the 2002 *R/V Marion Dufresne* cruise. Technical assistance was provided by K. Thompson, H. Berg and R. Petty at UCSB. The manuscript benefited from suggestions by A. Alldredge D. Lea, J. Hayes and two anonymous reviewers. This work has been supported by the U.S. National Science Foundation (OCE-0242041, Kennett; OCE-0447395, Valentine; IIS-0430835, Reddy) and UC Santa Barbara (Graduate Dissertation Fellowship to T. Hill). Contribution #XXXX from the Bodega Marine Laboratory, University of California, Davis.

Supplementary Information
Online Supplementary Information provides additional discussion and information on tar index, % tar, C/N analyses, and GCXGC analyses.

Conflict of interest statement
The authors declare that they have no conflicts of interest.

REFERENCES

1. Chappellaz, J., Barnola, J.M., Raynaud, D., Korotkevich, Y.S., Lorius, C. (1990). *Nature* **345,** 127-131.

2. Hornafius, J.S., Quigley, D., Luyendyk, B.P. (1999). *J. Geophys. Res.* **104,** 20,703-20,711.

3. Kvenvolden, K., Rogers, B. W. Abrams, M.A., Whelan, J.K. (2005). *Mar and Petrol Geology*. **22**, 579-590.

4. Eichhubl, P., Greene, H.G., Naehr, T., Maher, N. (2000). *J. Geochem. Expl.* **69-70,** 545-549.

5. Orphan, V.J., Hinrichs, K.-U., Ussler III., W., Paull, C.K., Taylor, L.T., Sylva, S.P., Hayes, J.M., Delong, E.F. (2001). *Appl. Environ. Microbiol.* **67,** 1922-1934.

6. Richmond, W.C., Cummings, L.J., Hamlin, S., Nagaty, M.E. (1979). *USGS Open File Report* **81-307.**

7. Greene, H.G., Murai, L.Y., Watts, P., Maher, N.A., Fisher, M.A., Paull, C.K., Eichhubl, P. (2006). *Natural Haz and Earth System Sci.* **6**, 63-88.

8. Leifer, I., Clark, J.F., Chen, R.F. (2000). *Geophys. Res. Lett.* **27**, 3711-3714.

9. Hostettler, F.D., Rosenbauer, R.J., Lorenson, T.D., Dougherty, J. (2004). *Org. Geochem.* **35**, 725-746.

10. Boles, J.R., Eichhubl, P., Garven, G., Chen, J. (2004.) *AAPG Bulletin* **88**, 947-970.

11. Kennett, J.P., Cannariato, K.G., Hendy, I.L., Behl, R.J. (2000). *Science* **288.** 128-133.

12. Hill, T.M., Kennett, J.P., Spero, H.J. (2003). *Mar. Micropaleontol.* **49**, 123-138.

13. Yamamoto, M., Yamamuro, M. Tada, R. (2000). *Proc. ODP, Sci. Results* **167**, 183-194.

14. Hendy, I.L., Kennett, J.P., Roark, E.B., Ingram, B.L. (2002). *Quat. Sci. Rev.* **21**, 1167-1184.

15. Behl, R.J., Kennett, J.P. (1996). *Nature* **379**, 243-246 (1996).

16. Hill,T. (2004). Ph.D. Thesis, University of California Santa Barbara.

17. Orr, W.L. (1986), *Organic Geochemistry* **10**, 499-516.

18. Crisp, P.T., Brenner, S., Venkatesan, M.I., Ruth, E., Kaplan, I.R. (1979). *Geoch. Cosmochim. Acta* **44**, 1791-1801.

19. Lorenson, T.D., Dougherty, J.A., Ussler III, W., Paull, C.K. (2003). *USGS Open File Rept.* **03-122**.

20. Luyendyk, B., Kennett, J., Clark, J.F. (2005). *Mar. Petrol. Geol.* **22**, 591-596

21. Boles, J.R., Clark, J.F., Leifer, I., Washburn, L. (2001). *J. Geophys. Res.* **106**, 27,077-27,086.

22. Clark, P. U., McCabe, A. M., Mix, A.C., Weaver, A. J. (2004). *Science* **304**, 1141-1144.

23. Behl, R.J. (1995). *Proc. Ocean Drilling Program*, Scientific Results **146**, 295-308.

24. Kvenvolden, K.A., McMenamin, M.A. (1980). *U.S. Geological Survey Circ.* **C825**, 11.

25. Sassen, R., Joye, S., Sweet, S.T., DeFreitas, D.A., Milkov, A.V., MacDonald, I.R. (1999). *Org. Geochem.* **30**, 485-497.

26. Chapman, R., Pohlman, J., Coffin, R., Chanton, J., Laphan, L. (2004). *EOS Trans. AGU* **85,** 361-365

27. Gorman, A. R., Holbrook, W.S., Hornbach, M.J., Hackwith, K.L., Lizarralde, D., Pecher, I. (2002). *Geology* **30**, 327-330.

28. Paull, C.K., Brewer, P.G., Ussler, W. III, Peltzer, E.T., Rehder, G., Clague, D. (2003). *Geo-Mar. Lett.* **22**, 198-203.

29. Kvenvolden, K.A. (1993). *Reviews of Geophysics.* 31 (2), 173-187.

30. Severinghaus, J. Brook, E. (1999). *Science* **286**, 930-933.

FIGURE CAPTIONS

1. Map of Santa Barbara Channel indicating MD02-2503 (570 m; 34.28N, 120.04W, adjacent to ODP Site 893) and MDO2-2504 (440 m; 34.23N, 119.86W) coring sites (hollow circles), collected in June 2002 from the *R/V Marion Dufresne*. Sedimentation rates at these locations averaged 130cm/ky. The location of previously described methane seepage sites (from hydrocarbon or gas hydrate reservoirs) are indicated by black circles; these seepage sites were inferred by the identification of active gas seepage, tar mounds, mud volcanoes, pockmarks, and/or authigenic carbonates, sometimes accompanied by *Beggiatoa*-like organisms (sulfide-oxidizing bacteria); seepage sites summarized from references 4-6. Areas of the gas hydrate stability zone are shaded for the Last Glacial Maximum and the Holocene (light blue-grey shading) and Termination IA (dark grey shading). Explanation of these scenarios and the estimates of gas hydrate stability are presented in the discussion and in Fig. 4. The total area of gas hydrate stability decreased during deglaciation, potentially destabilizing hydrates shown in the lighter blue-grey region. Map adapted from (4, 6, 7 and www.marine-geo.org/geomapapp/).

2. A) Tar index (blue) for MDO2-2503. B) $\delta^{18}O$ of *G. bulloides* (red) for MD02-2503. C) $\delta^{18}O$ of *G. bulloides* (red) for MD02-2504. D) Tar index (blue) for MD02-2504. Tar index reflects the % of sand grains composed of or coated by tar (e.g., 1=10%, 5= 50%). E) Lamination index for MD02-2503 (1= well laminated, 4= massive/bioturbated). The lamination index has been previously shown to change in concert with climatic changes recorded in the Greenland ice core (GISP2; 15). Isotopic data from (16). Location of

chronological tiepoints (to ODP 893; 14) denoted by diamonds. Major climatic intervals (Holocene, Terminations IA and IB) as well as Interstadials 2-5 are labeled.

3. The tar index (blue) and weight % tar (red, dashed line) covary in MD02-2503 between 15-14ka. Three distinct pulses (shaded) of tar abundance are recorded by the tar index and % tar, reaching maximum values of 4-5 in the tar index and 5-11% by weight (a 3-fold increase from background values).

4. Idealized gas hydrate stability model for the SBC during three separate intervals of the past ~25,000 years. Each box is of equal size, representing the deepest 250 m of the SBC. Scenarios refer to those described in the discussion and shown in Fig. 1. **Scenario 1**: Last Glacial Maximum (18 ka), with maximum basin depth of ~470m and bottom water temperatures of 2°C. **Scenario 2**: Termination IA (16-14 ka), when bottom water temperatures had warmed by ~2°C and sea level had risen by only 15m (maximum basin depth 485 m; 22). **Scenario 3**: Early Holocene (~9 ka), with basin near modern depth of 590m; bottom waters had warmed by an additional ~2°C. During scenarios 1 and 3, almost half of the deep SBC waters were within the gas hydrate stability field; in contrast, during scenario 2 (Termination 1A) the majority of the deep SBC was outside of the stability field, promoting instability of gas hydrates at shallower depths. This figure highlights the importance of temperature change (relative to sea level) in gas hydrate stability. Gas hydrate stability curve adapted from (29); estimates of bottom water temperature from (16).

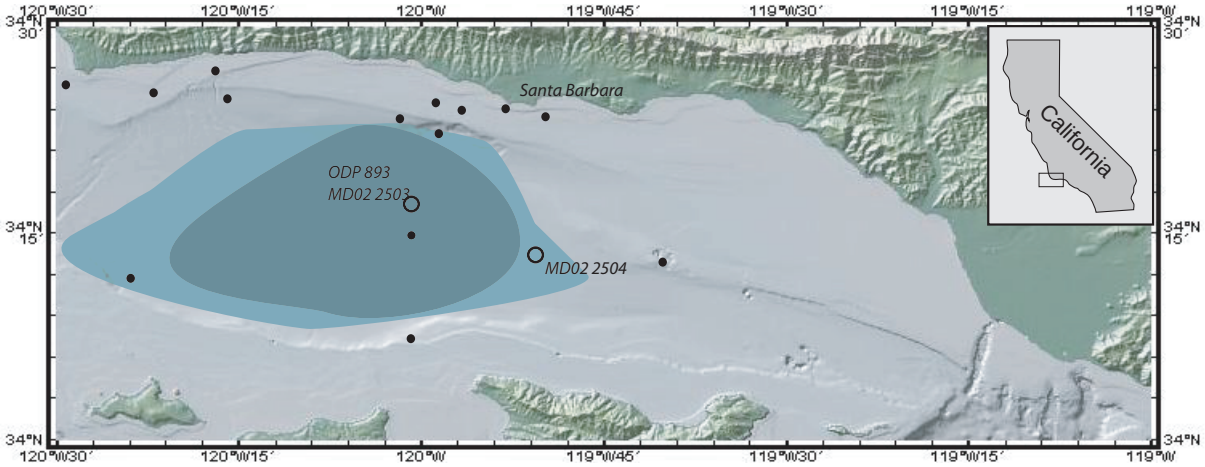
120°W30′
120°W15′
120°W
119°W45′
119°W30′
119°W15′
119°W
34°N 30′
34°N 15′
34°N
Santa Barbara
ODP 893
MD02 2503
MD02 2504
California

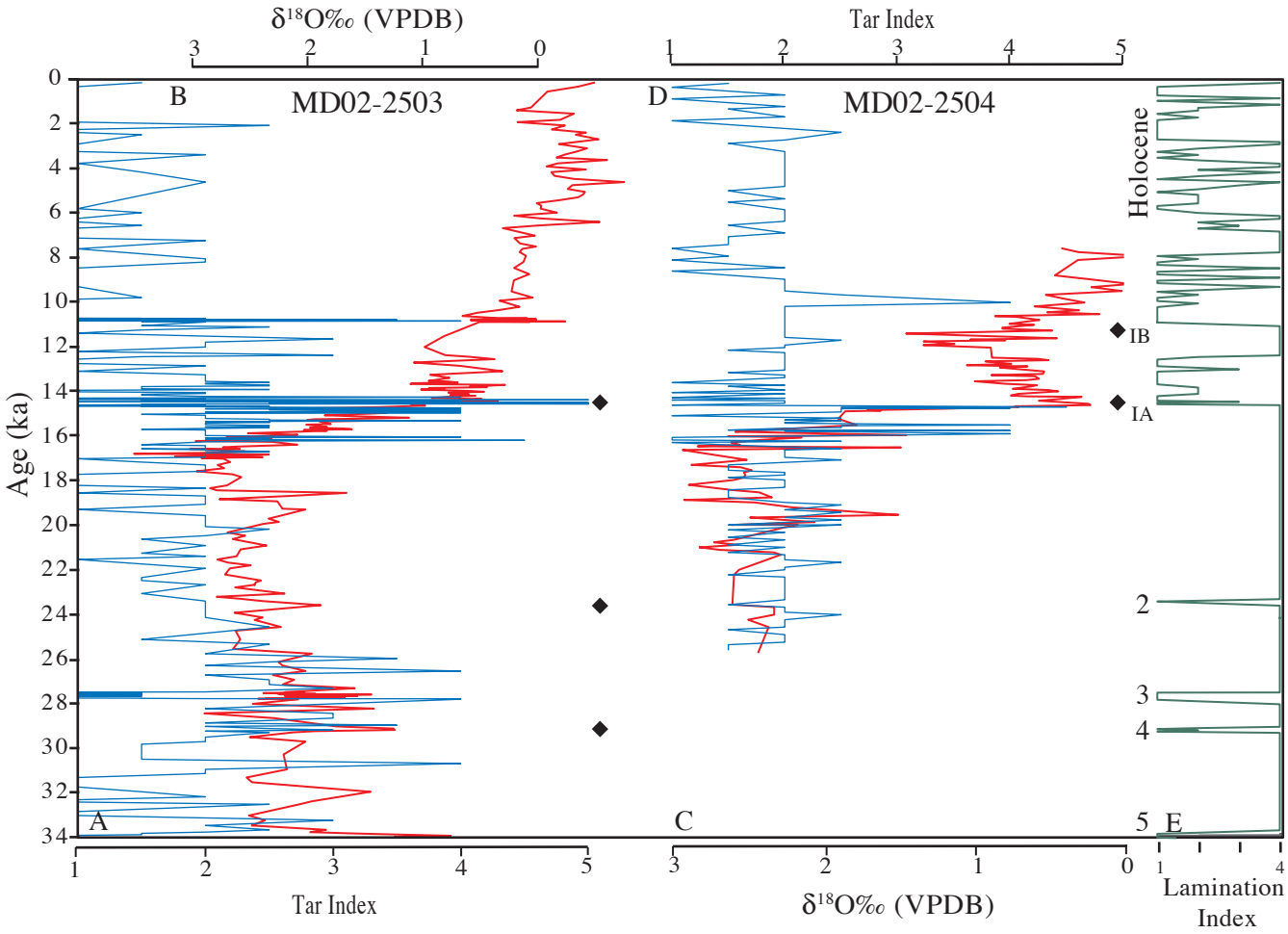
δ18O‰ (VPDB)
Tar Index
MD02-2503
MD02-2504
B
D
A
C
E
Age (ka)
Holocene
IB
IA
Tar Index
δ18O‰ (VPDB)
Lamination Index

Figure 2.

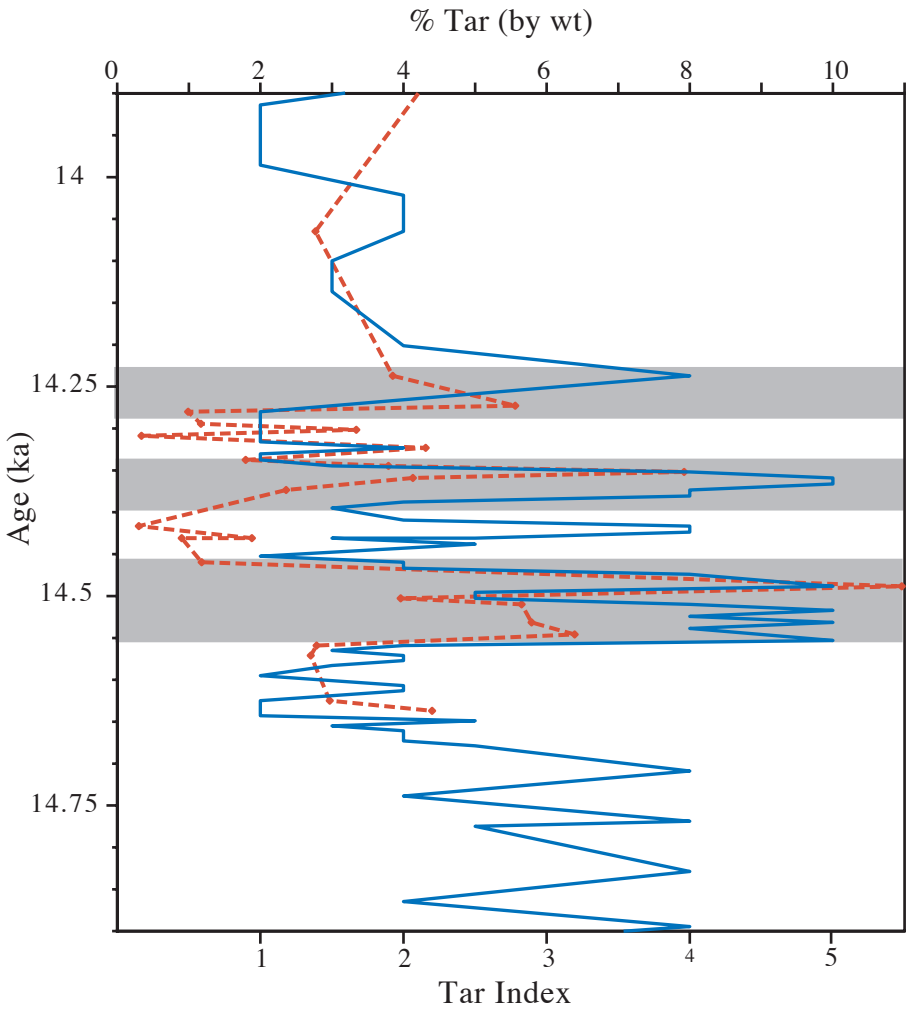

Figure 3.

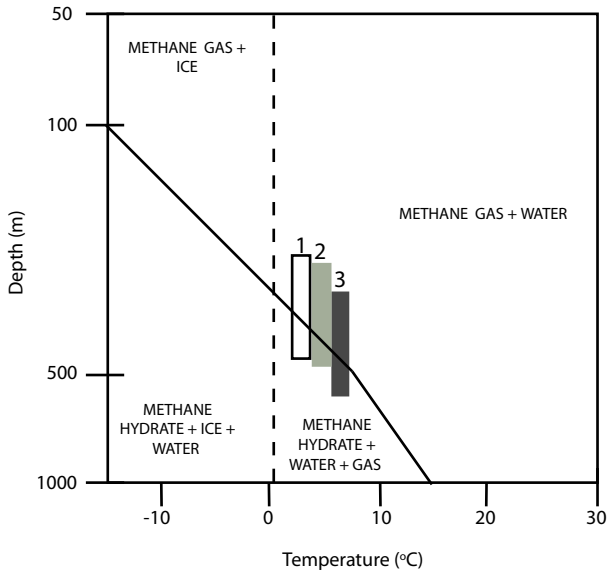
50
100
500
1000
Depth (m)
METHANE GAS + ICE
METHANE GAS + WATER
1
2
3
METHANE HYDRATE + ICE + WATER
METHANE HYDRATE + WATER + GAS
-10
0
10
20
30
Temperature (°C)